Clinical Neurophysiology 153 (2023) 33–45

Contents lists available at ScienceDirect

Clinical Neurophysiology

journal homepage: www.elsevier.com/locate/clinph

Functional and structural connectivity in the Papez circuit in different stages of Alzheimer's disease

Emre Hari [a,b,c,*], Gozde Kizilates-Evin [b,c], Elif Kurt [b,c], Ali Bayram [b,c], Cigdem Ulasoglu-Yildiz [b,c], Hakan Gurvit [c,d], Tamer Demiralp [c,e]

[a] Graduate School of Health Sciences, Istanbul University, 34216 Istanbul, Turkey
[b] Department of Neuroscience, Aziz Sancar Institute of Experimental Medicine, Istanbul University, 34093 Istanbul, Turkey
[c] Hulusi Behcet Life Sciences Research Laboratory, Neuroimaging Unit, Istanbul University, 34093 Istanbul, Turkey
[d] Department of Neurology, Behavioral Neurology and Movement Disorders Unit, Istanbul Faculty of Medicine, Istanbul University, 34093 Istanbul, Turkey
[e] Department of Physiology, Istanbul Faculty of Medicine, Istanbul University, 34093 Istanbul, Turkey

HIGHLIGHTS

- We examined the multimodal connectivity changes of the Papez circuit in Alzheimer's disease.
- The ventral cingulum is critical for the early detection of Alzheimer's disease.
- The functional connectivity between retrosplenial and parahippocampal cortices is affected early in the disease.

ARTICLE INFO

Article history:
Accepted 16 June 2023
Available online 30 June 2023

Keywords:
Alzheimer's disease
Magnetic resonance imaging
Functional connectivity
Diffusion tensor imaging
Multimodal neuroimaging

ABSTRACT

Objective: Alzheimer's disease (AD) is a progressive neurodegenerative continuum with memory impairment. We aimed to examine the detailed functional (FC) and structural connectivity (SC) pattern of the Papez circuit, known as the memory circuit, along the AD.
Methods: MRI data of 15 patients diagnosed with AD dementia (ADD), 15 patients with the amnestic mild cognitive impairment (MCI), and 15 patients with subjective cognitive impairment were analyzed. The FC analyses were performed between main nodes of the Papez circuit, and the SC was quantified as fractional anisotropy (FA) of the main white matter pathways of the Papez circuit.
Results: The FC between the retrosplenial (RSC) and parahippocampal cortices (PHC) was the earliest affected FC, while a manifest SC change in the ventral cingulum and fornix was observed in the later ADD stage. The RSC-PHC FC and the ventral cingulum FA efficiently predicted the memory performance of the non-demented participants.
Conclusions: Our findings revealed the importance of the Papez circuit as target regions along the AD.
Significance: The ventral cingulum connecting the RSC and PHC, a critical overlap area between the Papez circuit and the default mode network, seems to be a target region associated with the earliest objective memory findings in AD.
© 2023 International Federation of Clinical Neurophysiology. Published by Elsevier B.V. All rights reserved.

1. Introduction

Alzheimer's disease (AD) is a neurodegenerative process typically expressed with subjective memory complaints and continues with progressive memory impairment, spreading to multiple cognitive domains leading to dementia. When the functional impairment threshold in the disease course is exceeded, it corresponds to the AD dementia (ADD) stage, divided into sub-stages as mild, moderate, and severe (Molinuevo et al., 2017). The transitional stage between the subjective memory impairment (SCI) and dementia threshold is called the mild cognitive impairment (MCI) stage or prodromal AD (Roberts et al., 2008). The AD process starts with a preclinical stage, during which only the pathological features of the disease evolve for many years before the clinical

* Corresponding author.
E-mail addresses: emrehr@hotmail.com (E. Hari), gozde.kizilates@gmail.com (G. Kizilates-Evin), elifkurt@istanbul.edu.tr (E. Kurt), ali.bayram@istanbul.edu.tr (A. Bayram), cigdemulasoglu@gmail.com (C. Ulasoglu-Yildiz), gurvit@istanbul.edu.tr (H. Gurvit), demiralp@istanbul.edu.tr (T. Demiralp).

https://doi.org/10.1016/j.clinph.2023.06.008
1388-2457/© 2023 International Federation of Clinical Neurophysiology. Published by Elsevier B.V. All rights reserved.

symptoms appear. Neuroimaging studies reveal that changes in brain structure are already advanced by the time ADD is diagnosed, emphasizing the need to examine the early stages of the disease (Filippini et al., 2009; Supekar et al., 2008).

The main neuropathological changes that cause neurodegeneration in AD are the accumulation of amyloid-beta (Aβ) plaques in the neural parenchyma and hyperphosphorylated tau protein in the form of neurofibrillary tangles (NFTs) accumulating inside the neuron (Sanabria-Castro et al., 2017). In addition, both Aβ plaques and NFTs are the final stages of the oligomerization process. Amyloid-beta plaques appear in the neocortex, primarily in the midline structures, and progress towards the limbic structures (Hampel et al., 2021; Villemagne et al., 2011). NFTs, on the other hand, progress trans-synaptically, starting from Layer II of the entorhinal cortex (ERC), first to the hippocampal and paralimbic structures, then to the neocortical areas (Braak and Braak, 1995, 1991; Braak and Del Tredici, 2012).

The hippocampus has long been the center of memory research, as it is strongly associated with AD neuropathology. However, growing evidence has shown that episodic memory does not rely solely on the hippocampus, as other cortical and subcortical structures also play critical roles (Acosta-Cabronero and Nestor, 2014; Aggleton, 2014; Aggleton et al., 2016; Jankowski et al., 2013). As has been shown by several studies (Aggleton et al., 2022; Bubb et al., 2017; Choi et al., 2019; Papez, 1937) the Papez circuit consisting of hippocampal formation (HF), parahippocampal cortex (PHC), ERC, mammillary bodies, anterior thalamic nuclei (ATN), cingulate cortex and retrosplenial cortex (RSC) hubs constitutes a large-scale network in a strategic and important location of the telencephalon. Posterior cingulate cortex (PCC) and RSC complex also comprises the posterior hub of the default mode network (DMN), one of the main intrinsic connectivity networks (ICNs) that has been associated with Alzheimer's disease continuum (ADC) (Greicius et al., 2004; Pievani et al., 2014). The DMN displaying coherent low-frequency oscillations at rest between the PCC/RSC complex and other nodes in the ventromedial prefrontal cortex, bilateral inferior parietal lobules, and superior temporal sulci is thought to focus on internal mental processes such as self-referential processing, autobiographical memory, and recall (Andrews-Hanna et al., 2010; Raichle et al., 2001; Staffaroni et al., 2018).

The increasing evidence for the importance of interregional connectivity in the spread of neuropathologies in AD gave rise to a new concept called the network degeneration hypothesis (Chételat, 2018; Wang et al., 2015). In this context, beyond the functional connectivity (FC) changes, the basic white matter pathways also emerge as important features of the disease progression (La Joie et al., 2014; Raj et al., 2012; Seeley et al., 2009; Teipel et al., 2016). In diffusion tensor imaging studies, the integrity of the fibers with direct connections to the medial temporal lobe structures, including the cingulum bundle, fornix, perforant pathway, and uncinate fascicle are reported to be impaired in AD (Kalus et al., 2006; Sexton et al., 2010; Zhang et al., 2007). The first microstructural changes in these pathways appear years before individuals develop cognitive deficits. It is not unequivocally shown whether FC changes precede or follow these structural connectivity (SC) changes (Fletcher et al., 2013; Zhuang et al., 2012).

Within the scope of the network degeneration hypothesis, most of the previous studies on ADC have focused on ICNs, and mostly on the DMN, that have appeared in empirical analysis of the whole brain connectivity studies (Badhwar et al., 2017; Golchert et al., 2017; Greicius et al., 2004; Pievani et al., 2014; Supekar et al., 2008; Teipel et al., 2016). On the other hand, from a historical perspective, the Papez circuit as a core circuitry associating the medial temporal lobe structures with the neocortical areas in the context of episodic memory, is an important concept in memory research. Assuming that a detailed investigation of the FC and SC changes between the components of the Papez circuit and of its connections with other large-scale cognitive networks can improve our understanding about the connectivity changes in ADC, this study aims to examine both the SC and FC changes of the Papez circuit in association with the spread pattern of neuropathologies along the ADC. For the Papez circuit, the main white matter pathways are the fornix and the cingulum bundle, which in neuroimaging studies showed associations with impaired episodic memory function (Catani et al., 2013; Fellgiebel et al., 2008; Huang and Auchus, 2007; Papez, 1937; Sexton et al., 2010). There are also a range of neuroimaging studies associatied with the ADC on both anatomical and FC changes of the sub-fields of the HF and various medial temporal lobe components that are part of the Papez circuit (Badhwar et al., 2017; Forno et al., 2021). However, an SC or FC study that bases the analyses specifically on the Papez circuit is missing, and we believe that such conceptualization might be helpful in following the progression of the neuropathological and cognitive processes especially in the early phases of the disease continuum and hence in defining possible biomarkers for the early diagnosis of the disease. Therefore, we investigated systematically the SC and FC changes within the Papez circuit, by also taking the connections with other more studied ICNs into consideration.

2. Methods

2.1. Participants

Forty-five voluntary participants were recruited from the outpatient clinic of the Behavioral Neurology and Movement Disorders Unit at the Department of Neurology of Istanbul Faculty of Medicine. All participants underwent a standardized clinical interview by experienced behavioral neurologists. All participants were assessed using the Turkish version of the Mini-Mental State Examination (MMSE) (Folstein et al., 1975), Clinical Dementia Rating scale (CDR) (Morris, 1993), and Free and Cued Selective Reminding Test (FCSRT) (Buschke, 1984; Ivnik et al., 1997). The test scores, in addition to clinical evaluation, were used to determine the three groups. Accordingly, 15 subjects with early-stage ADD, 15 with amnestic MCI, and 15 with SCI participated in the study. For the ADD group, patients were diagnosed according to the National Institute on Aging-Alzheimer's Associations (NIA-AA) criteria (McKhann et al., 2011). For the memory score used in the diagnosis of the MCI group, the threshold value with a high probability of conversion to AD was preferred (Grober et al., 2010; Saka et al., 2006). The MCI group consisted of individuals diagnosed with MCI according to Petersen criteria, by assigning the subjects with the total free recall (TFR) scores of the FCSRT $\leq$24 to the MCI group (Grober et al., 2010; Petersen, 2004; Saka et al., 2006). Lastly, subjects who had subjective memory complaints with a CDR score of 0 and an FCSRT-TFR score higher than 24 were defined as the SCI group. Any other neurological and psychiatric disorders and any contraindication for MRI were set as exclusion criteria (Jessen et al., 2014; Lemos et al., 2015; Saka et al., 2006; Teichmann et al., 2017).

2.2. MRI acquisition

The structural and functional MRI images were acquired at Hulusi Behcet Life Sciences Research Laboratory, Istanbul University, using a 3 Tesla MRI system (Phillips, Achieva, Best, The Netherlands) equipped with a 32-channel SENSE head coil. T1-weighted anatomical images were recorded with 3D TFE (Turbo Field Echo) sequence in the axial plane (the anterior commissure – posterior commissure aligned) with the following parameters:

Total scan time: 5 minutes 55 seconds, time of repetition (TR): 8.3 ms, time of echo (TE): 3.8 ms, flip angle: 8°, field of view (FOV): 220 × 240 mm, voxel size: 1 mm^3 (isotropic) and 180 axial slices. Resting-state functional magnetic resonance imaging (rs-fMRI) data were recorded with echo-planar imaging (EPI) sequence in the axial plane (anterior commissure-posterior commissure aligned) with the following parameters: TR: 3000 ms, TE: 30 ms, flip angle: 80°, FOV: 212 × 199 mm, voxel size: 3.31 × 3.31 × 3.31 mm, acquisition matrix size: 64 × 59. Following 5 dummy volumes, 195 volumes, each containing 48 axial slices covering the whole brain, were obtained with a total scan time of 10 minutes. All participants were instructed to remain awake, lie in the most relaxed position with closed eyes, and not focus on anything. Diffusion tensor imaging (DTI) data were obtained using a single-shot, multi-shell EPI sequence with the following parameters: TR: 9032 ms, TE: 92 ms, flip angle: 90°, FOV: 200 × 236 mm, voxel size: 2.08 × 2.11 × 2.27 mm, and acquisition matrix size: 88 × 104. Each volume contained 71 straight axial slices covering the whole brain. In addition to the $b = 0$ image, DTI data were recorded with 4 different b values for a total of 120 diffusion directions (60 directions with $b = 3000$ s/mm^2, 46 directions with $b = 1000$ s/mm^2, seven directions with $b = 200$ s/mm^2, six directions with $b = 100$ s/mm^2).

2.3. Functional connectivity analysis

2.3.1. Segmentation and parcellation of structural data

The critical structures of the Papez circuit known to be structurally and functionally connected were selected as target regions of interest (ROIs) for the FC analysis. The FreeSurfer software, version 6.0.0 (https://surfer.nmr.mgh.harvard.edu), which performs segmentation and parcellation in subjects-space, was used to analyze structural data (Dale et al., 1999; Fischl et al., 2002, 2001). After the cortical parcellation process, individual cortical parcels were obtained based on the Destrieux atlas (Destrieux et al., 2010). The ROIs are listed as the anterior part of the cingulate gyrus and sulcus (Anterior cingulate cortex-ACC), the posterior-dorsal part of the cingulate gyrus (Posterior cingulate cortex-PCC), the isthmus of the cingulate gyrus (Retrosplenial cortex-RSC), and the parahippocampal part of the medial occipito-temporal gyrus (Parahippocampal cortex-PHC) including the entorhinal cortex (ERC). Fig. 1A displays the cortical parcels selected as target ROIs in a representative participant.

After the HF segmentation, individual hippocampal subregions were obtained using an HF atlas created using ultra-high resolution magnetic resonance images (Iglesias et al., 2015). Among the hippocampal subregions, CA1, CA3, subiculum (SUB), and dentate gyrus (DG) (Fig. 1B) were selected as target ROIs (Jankowski et al., 2013).

Finally, the thalamic segmentation was conducted, and individual thalamic nuclei were obtained from the thalamic atlas, which was created based on histological data (Iglesias et al., 2018). In order to form ATN, anteroventral, anteromedial, anterodorsal, and laterodorsal nuclei (Fig. 1C) were combined into a single target ROI of the anterior thalamic nuclei group (Iglesias et al., 2018; Krauth et al., 2010). In addition, individual white matter (WM) and cerebrospinal fluid (CSF) masks were obtained, which were used for regressing out the non-specific BOLD fluctuations in functional analyses.

In summary, nine target ROIs related to the Papez circuit and Alzheimer's disease were paired based on the well-known functional and structural connections within the Papez circuit (Fig. 2) (Aggleton et al., 2016; Bubb et al., 2017; Catani et al., 2013; Honda and Shibata, 2017; Jankowski et al., 2013; Papez, 1937; Schultz and Engelhardt, 2014).

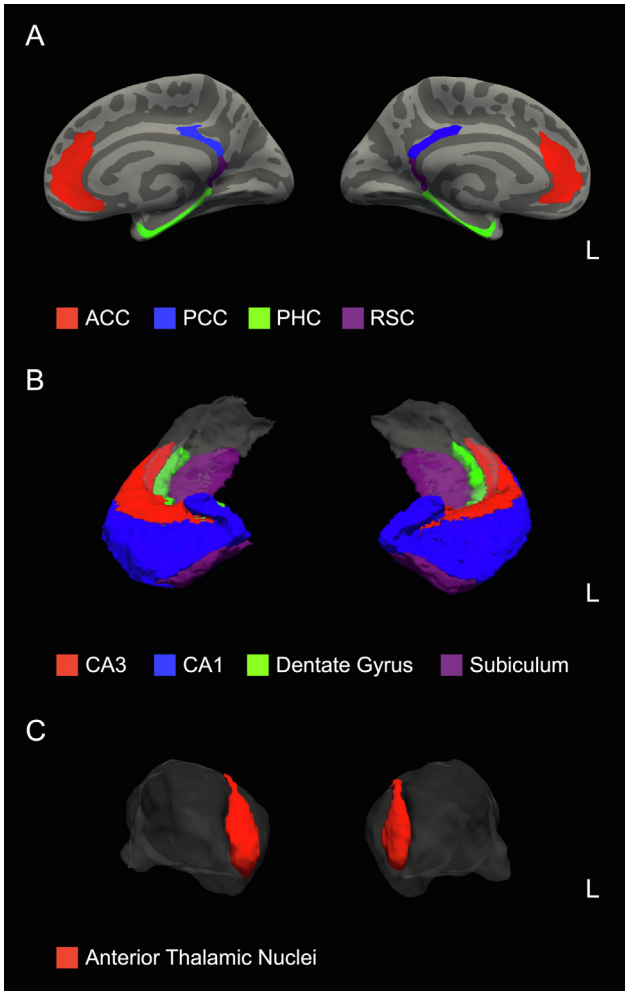


Fig. 1. Region of interest localization in a representative participant. (A) Cortical parcels. (B) Hippocampal subregions. (C) Anterior thalamic nuclei. *L*: Left; *ACC*: Anterior cingulate cortex; *PCC*: Posterior cingulate cortex; *RSC*: Retrosplenial cortex; *PHC*: Parahippocampal cortex; *CA*: Cornu Ammonis.

2.3.2. Analysis of resting-state fMRI data

The ROI-to-ROI analyses among selected Papez circuit regions were performed using the FSL (Functional Magnetic Resonance Imaging of the Brain's Software Library) v6.0.3 (https://fsl.fmrib.ox.ac.uk/fsl/fslwiki/FSL) software package (Smith et al., 2004). The calculation of the rotation and translation parameters of the participants and the movement correction were performed using FEAT (FMRI Expert Analysis Tool) v6.00 (Jenkinson et al., 2002). Functional data were registered to the high-resolution structural data of each subject using FLIRT (FMRIB's Linear Image Registration Tool), and transformation matrices were stored (Jenkinson et al., 2002; Jenkinson and Smith, 2001).

After the registration process, individual WM and CSF masks were transferred into functional data space and binarized (WM threshold 0.9 and CSF threshold 0.5) to extract the BOLD time-series of WM and CSF. Motion parameters, WM, and CSF time series were defined as nuisance variables and regressed out from the functional data using FEAT. Then a band-pass filter of 0.01–0.1 Hz was applied to the functional data to filter out effects from noise sources. The filtered functional data were transferred to the anatomical space using the transformation matrices. Finally, time-series of individual target ROIs were extracted from functional data for connectivity analysis.

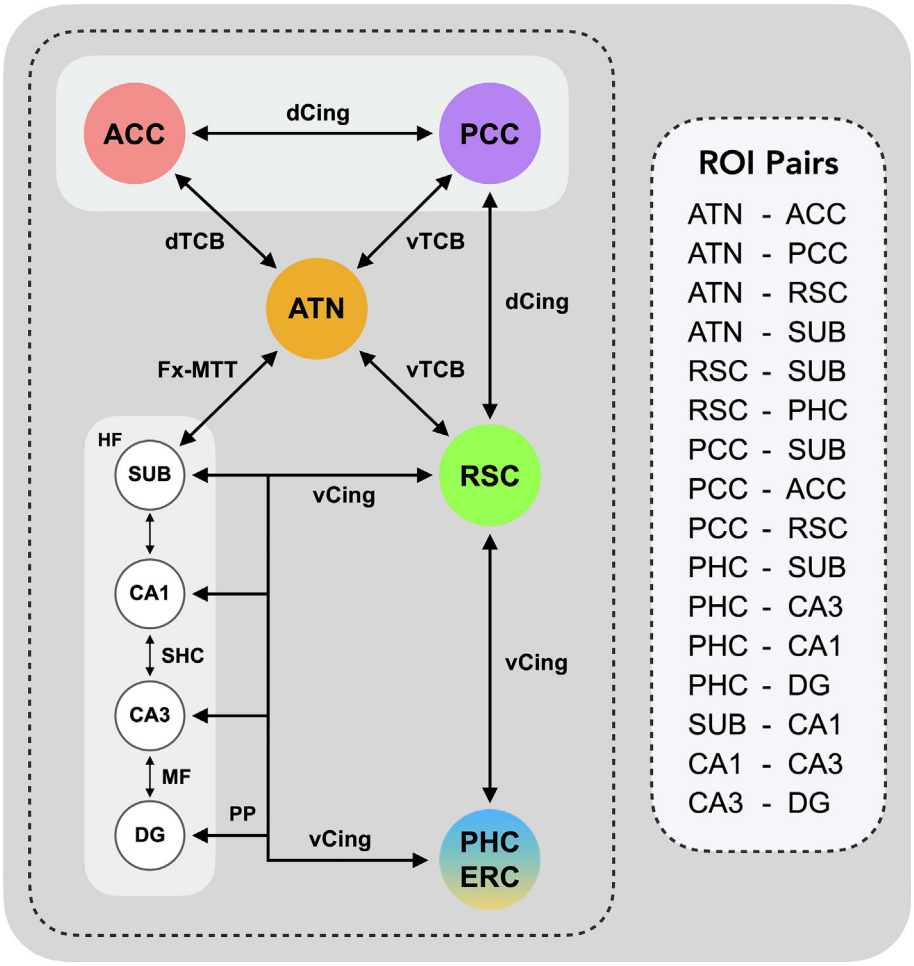


Fig. 2. Regions of interest pairs were created based on functional and structural connections. *ATN*: Anterior Thalamic Nuclei; *ACC*: Anterior Cingulate Cortex; *PCC*: Posterior Cingulate Cortex; *RSC*: Retrosplenial Cortex; *PHC*: Parahippocampal Cortex; *ERC*: Entorhinal Cortex; *DG*: Dentate Gyrus; *CA*: Cornu Ammonis; *HF*: Hippocampal Formation; *vCing*: Ventral cingulum; *dCing*: Dorsal cingulum; *vTCB*: Ventral thalamo-cingulate bundle; *dTCB*: Dorsal thalamo-cingulate bundle; *Fx*: Fornix; *MTT*: Mamillo-thalamic tract; *PP*: Perforant pathway; *MF*: Mossy fibers; *SHC*: Schaffer collaterals; *ROI*: Region of Interest.

Pearson correlation analysis was performed for each ROI pair using customized Python code (Python version 2.7.7 (https://www.python.org) with Numpy and Nibabel modules). Correlation values were converted using Fisher's r-to-z transform.

For between-group comparisons, the Kruskal-Wallis H test and for pairwise comparisons the Mann-Whitney U test were used in R version 4.0.0 (https://www.R-project.org). In order to increase the robustness of the FC analyses, the Monte Carlo permutation tests with 10,000 iterations were used, and the false discovery rate (FDR) correction was applied for multiple comparisons using the P.adjust function in R (version 4.0.0, https://www.R-project.org) (Benjamini and Hochberg, 1995; Genovese et al., 2002; Hothorn et al., 2008). The significance threshold was determined as $p_{FDR\text{-}corr} < 0.05$ for the Kruskal-Wallis H test and post-hoc analyses. Eta-squared values were calculated for all results as shown in the Appendix (Tables A1 and A2). For displaying the effect sizes, the eta-square values of all results were calculated and shown in the Appendix (Tables A1 and A2) (Tomczak and Tomczak, 2014).

2.4. Structural connectivity analysis

Analysis of DTI data was also performed using FSL software (version 6.0.3) (Smith et al., 2004). First, non-brain tissues from the b0 image were deleted with BET (Brain Extraction Tool) (Smith, 2002). Next, eddy currents and subjects' head motions were corrected using *eddy_correct* in FMRIB's Diffusion Toolbox (FDT) (Andersson and Sotiropoulos, 2016). Fractional anisotropy (FA) maps were created by fitting a tensor model to the eddy-corrected diffusion data using FDT's *dtifit* function.

All subjects' FA data were aligned into $1 \times 1 \times 1$ mm MNI space using the non-linear registration tool (FNIRT) (Smith et al., 2004). The mean FA skeleton, representing the centers of all tracts common to the group, was derived from the mean FA data using an FA thresholded of 0.2. ROI-restricted Tract-Based Spatial Statistics (TBSS) (Smith et al., 2006) analysis of the FA data was performed using the five ROIs corresponding to the main white matter tracts of the Papez circuit: fornix, left and right dorsal cingulum, and left and right ventral cingulum (Fig. 3) (Catani et al., 2013; Papez, 1937).

Template regions of these structures were selected using Johns Hopkins University white matter atlas (JHU ICBM-DTI-81) and multiplied with the mean FA skeleton mask to construct target ROIs (Hubbard et al., 2018). Non-parametric permutation inference with 10,000 iterations and threshold-free cluster enhancement (TFCE) procedure were applied to correct for multiple comparisons (Smith and Nichols, 2009; Winkler et al., 2014). After a one-way analysis of variance (ANOVA) among the three patient subgroups, post-hoc analyses for the significant clusters found in the ANOVA were performed between pairs of groups using t-tests. False discovery rate (FDR) correction was applied to all results

using the P.adjust function in R for multiple comparisons (Benjamini and Hochberg, 1995; Genovese et al., 2002; Hothorn et al., 2008). The significance threshold was set at $p_{FDR\text{-}corr} < 0.05$ for ANOVA and post-hoc analyses. In addition, effect sizes (ANOVA: partial eta-squared and t-test: Cohen's d) were calculated (Tomczak and Tomczak, 2014).

2.5. Multimodal evaluation of the functional and structural connectivities

In order to complement the results of the multi-group comparisons carried out separately on the FC and SC data into multimodal classification models that best discriminate the disease stages, linear discriminant analyses (LDA) were performed by including both the FCs and SCs, that significantly differed in the multi-group comparisons, in the discriminant function with the stepwise approach. Assuming that the critical connectivity features for the different stages of the disease correspond to distinct portions of the Papez circuit, we performed separate LDA for each pair of the disease stages. The stepwise approach revealed the most discriminative feature set for each disease stage. The significance threshold of the discriminant analysis was set at $p < 0.017$ (Bonferroni corrected for the number of runs, 0.05/3).

Finally, a forward stepwise multiple linear regression analysis was performed on non-demented participants (SCI + MCI groups) in order to identify possible connectivity predictors of a progressive memory decline expressed in FCSRT-TFR scores before the occurrence of a strong change in the ADD group. To be able to observe any associations with those connectivity metrics that may show a progressive change along the non-demented participants but could not survive the between-group comparisons, all investigated FCs (32 ROI pairs) and SCs (five ROIs) were included in the regression analysis.

2.6. Statistical analyses on demographic and clinical data

Statistical analyses on the demographic, clinical and neuropsychological variables were carried out using R version 4.0.0 (https://www.R-project.org). Shapiro-Wilk test was used to examine the distributions, and one-way ANOVA was performed for normally distributed data followed by post-hoc comparisons. For non-normal distributed data, the Kruskal-Wallis H test was used with post-hoc analyses based on the Mann-Whitney U test. The Chi-square test was used to compare gender distribution across the subjects. The statistical significance threshold was $p < 0.05$ for all tests.

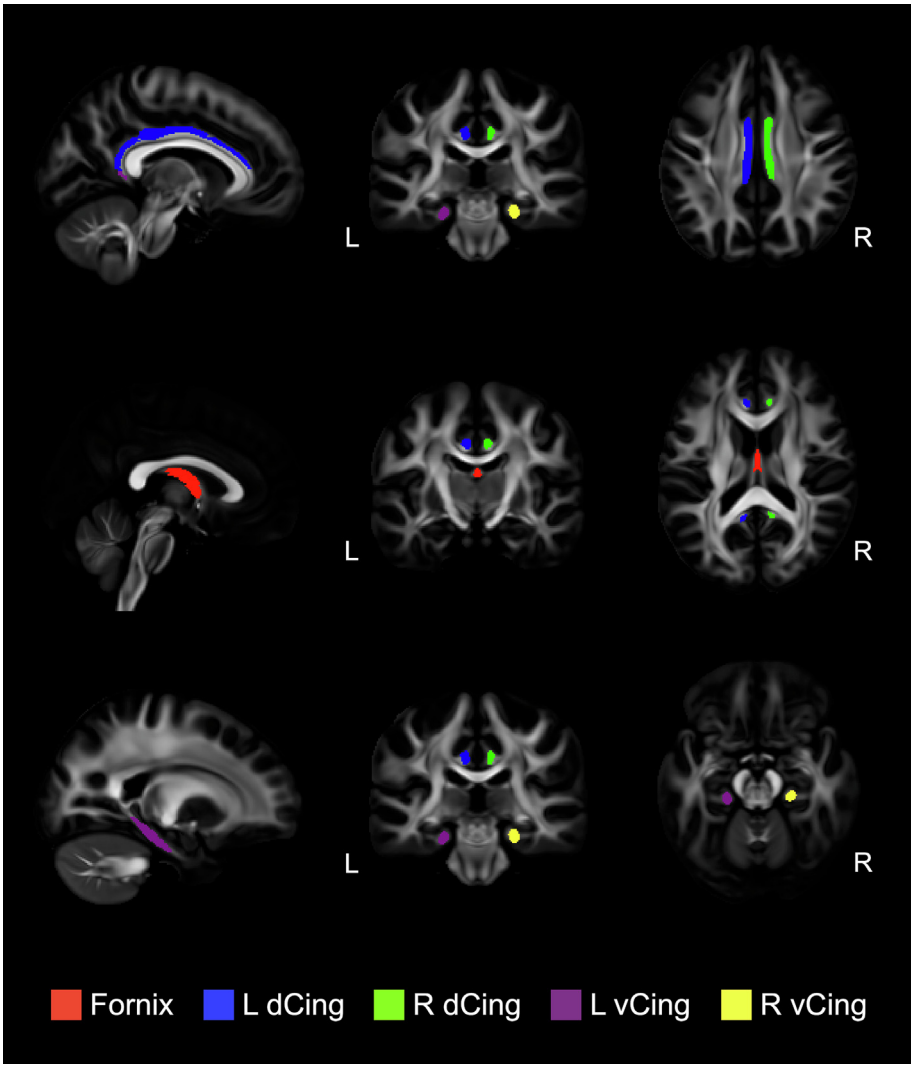


Fig. 3. Johns Hopkins University (JHU) white matter tracts were used for region of interest (ROI)-restricted TBSS analysis. Each target structure (Fornix, dCing: Dorsal cingulum, vCing: Ventral cingulum) is displayed as a color-coded ROI. *L*: Left; *R*: Right.

3. Results

3.1. Demographic and clinical results

The demographic and clinical profiles of the groups are shown in Table 1. There were no significant differences between the sub-groups regarding age, gender, and education. According to the Kruskal-Wallis test results, a significant difference was found between the groups in MMSE scores (χ^2 = 26.358, p < 0.001). Results of the pairwise comparisons showed that the MMSE scores of the SCI group were higher than those of both the MCI (p = 0.044) and ADD (p < 0.001) groups and the MMSE scores of the MCI group were higher than those of the ADD group (p = 0.019).

For the evaluation of objective memory impairment, FCSRT-TFR scores were analyzed using the Kruskal-Wallis H test, and a significant difference was found between the groups (χ^2 = 34.134, p < 0.001). The FCSRT-TFR scores of the SCI group were higher than those of the MCI (p < 0.001) and ADD (p < 0.001) groups, and the FCSRT-TFR scores of the MCI group were higher than those of the ADD group (p < 0.001).

3.2. Functional connectivity results

The comparisons of the FC values among the three groups showed significant differences in the left PHC – CA1 (χ^2 = 9.513, $p_{FDR\text{-}corr}$ = 0.048, η^2 = 0.131), left RSC – SUB (χ^2 = 9.190, $p_{FDR\text{-}corr}$ = 0.048, η^2 = 0.124), right PHC – RSC (χ^2 = 10.252, $p_{FDR\text{-}corr}$ = 0.048, η^2 = 0.149) and right PCC – ACC (χ^2 = 9.169, $p_{FDR\text{-}corr}$ = 0.048, η^2 = 0.123) connectivities (Fig. 4).

In pairwise comparisons of significant ROI pairs, a difference was found between ADD and SCI in left RSC – SUB (U = 42, $p_{FDR\text{-}corr}$ = 0.009, η^2 = 0.534), right PHC – RSC (U = 44, $p_{FDR\text{-}corr}$ = 0.009, η^2 = 0.519), left PHC-CA1 (U = 54, $p_{FDR\text{-}corr}$ = 0.026, η^2 = 0.443), and right PCC – ACC (U = 43, $p_{FDR\text{-}corr}$ = 0.009, η^2 = 0.526) pairs. A statistically significant difference was found between the ADD and MCI groups in the left PHC – CA1 (U = 44, $p_{FDR\text{-}corr}$ = 0.009, η^2 = 0.519) pair. Finally, a statistically significant difference was found in the right PHC – RSC (U = 49, $p_{FDR\text{-}corr}$ = 0.015, η^2 = 0.481) pair between the MCI and SCI groups. The statistically significant ROI pairs are shown in Fig. 4. Functional connectivity analysis results are given in detail in the Supplementary Material (Appendix Tables A1 and A2).

3.3. Structural connectivity results

ROI-restricted TBSS analysis revealed significant FA differences for fornix (F = 15.11, $p_{FDR\text{-}corr}$ = 0.015, partial η^2 = 0.245), right ventral cingulum (F = 12.02, $p_{FDR\text{-}corr}$ = 0.010, partial η^2 = 0.257) and left ventral cingulum (Cluster 1: F = 5.42, $p_{FDR\text{-}corr}$ = 0.045, partial η^2 = 0.213; cluster 2: F = 4.40, $p_{FDR\text{-}corr}$ = 0.045, partial η^2 = 0.165; cluster 3: F = 6.55, $p_{FDR\text{-}corr}$ = 0.042, partial η^2 = 0.201) among groups (Table 2, Fig. 5).

In post-hoc comparisons, FA displayed significant decrease in ADD compared with both MCI and SCI in fornix (ADD vs MCI: t = -3.69, $p_{FDR\text{-}corr}$ = 0.006, Cohen's d = 0.564; ADD vs SCI: t = -3.39, $p_{FDR\text{-}corr}$ = 0.006, Cohen's d = 0.531), right ventral cingulum (ADD vs MCI: t = -3.36, $p_{FDR\text{-}corr}$ = 0.006, Cohen's d = 0.522; ADD vs SCI: t = -3.81, $p_{FDR\text{-}corr}$ = 0.006, Cohen's d = 0.571) and left ventral cingulum cluster 1 (ADD vs SCI: t = -3.44, $p_{FDR\text{-}corr}$ = 0.006, Cohen's d = 0.533), left ventral cingulum cluster 2 (ADD vs SCI: t = -2.83, $p_{FDR\text{-}corr}$ = 0.019, Cohen's d = 0.461) and left ventral cingulum cluster 3 (ADD vs MCI: t = -2.80, $p_{FDR\text{-}corr}$ = 0.019, Cohen's d = 0.458; ADD vs SCI: t = -3.19, $p_{FDR\text{-}corr}$ = 0.007, Cohen's d = 0.506) (Fig. 5).

3.4. Multimodal evaluation of the functional and structural connectivity results

To complement the multi-group comparisons on the FC and SC variables, a multimodal classification was carried out by using stepwise LDA on both FC and SC variables that significantly differed among the three groups. The cross-validated results of the stepwise LDA carried out on pairs of disease stages revealed that the left PHC – CA1 (Standardized Canonical Discriminant Function Coefficients [SCDFC] = 0.896) and fornix (SCDFC = 1.021) discriminated the MCI and ADD groups with a high accuracy (Accuracy = 83.3%, Wilks' λ = 0.430, χ^2 = 22.815, eigenvalue = 1.328, canonical correlation = 0.755, p < 0.001). Additionally, the right PHC – RSC (SCDFC = 0.681) and right ventral cingulum (SCDFC = 0.761) discriminated the SCI and ADD groups with the same accuracy (Accuracy = 83.3%, Wilks' λ 0.509, χ^2 = 18.222, eigenvalue = 0.964, canonical correlation = 0.701, p < 0.001). Finally, the right PHC – RSC (SCDFC = 1) discriminated MCI group from the SCI group with a lower accuracy (Accuracy = 70%, Wilks' λ = 0.776, χ^2 = 6.957, eigenvalue = 0.288, canonical correlation = 0.473, p = 0.008). ROC curves for each discriminant analysis are given in the Appendix Fig. A1.

Finally, the forward stepwise multiple linear regression analysis carried out on the non-demented (SCI + MCI) participants by including all FC and SC variables as potential regressors revealed that the mean FA of the right ventral cingulum and the FC between the right PHC and RSC efficiently predicted the memory scores as measured with the FCSRT-TFR. In order to visualize these regressions, the correlations between each of the two variables and the FCSRT-TFR scores are depicted in Fig. 6. The model (R = 0.575, R^2 = 0.330, df = 2, F = 6.993, p = 0.004) explained 28.1% variance of the memory performance.

4. Discussion

This study investigated FC and SC differences within the Papez circuit among ADD, MCI, and SCI participants. Significant FC decreases among the three groups were detected between the circuit components (left PHC – CA1, RSC – SUB, and right PCC – ACC and PHC – RSC). The pattern of FC changes observed in the ANOVA

Table 1
Demographic and clinical characteristics of the groups.

	Mean ± SD			Test	p
	SCI (n = 15)	MCI (n = 15)	ADD (n = 15)		
Age	61.93 ± 7.71	67.00 ± 8.79	68.40 ± 8.60	F = 2.157*	0.128
Gender (F/M)	9 / 6	6 / 9	6 / 9	χ^2 = 1.607†	0.448
Education	13.40 ± 3.25	10.20 ± 3.95	10.67 ± 4.08	χ^2 = 5.320‡	0.070
MMSE	29.57 ± 0.85	28.00 ± 1.53	23.87 ± 3.62	χ^2 = 26.358‡	<0.001
FCSRT-TFR	29.78 ± 1.33	16.93 ± 1.22	6.93 ± 2.01	F = 56.363*	<0.001

F: Female; *M*: Male; *SD*: Standard deviation; *MMSE*: Mini-Mental State Examination; *FCSRT-TFR*: Free and Cued Selective Reminding Test-Total Free Recall; *SCI*: Subjective cognitive impairment; *MCI*: Mild cognitive impairment, *ADD*: Alzheimer's disease dementia; *One-way ANOVA; †Chi-square test; ‡Kruskal-Wallis H test. The significance threshold was set at p < 0.05.

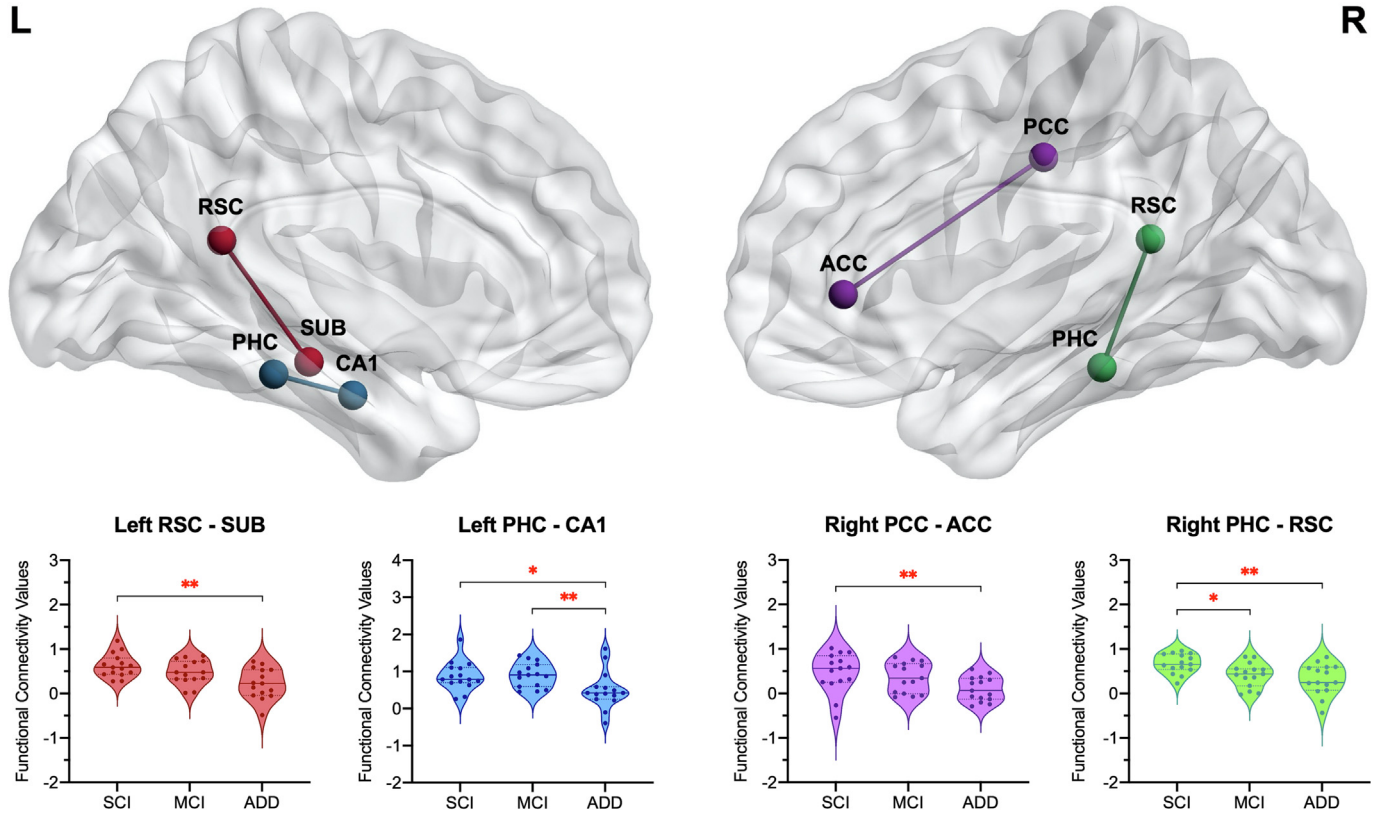


Fig. 4. Regions of interest pairs that show a significant difference (Kruskal-Wallis analysis) are shown using a 3D glass brain in MNI space (BrainNet Viewer, Xia et al., 2013). Red: Retrosplenial Cortex-Subiculum, blue: Parahippocampal Cortex-CA1, violet: Posterior Cingulate Cortex-Anterior Cingulate Cortex, and green: Retrosplenial Cortex-Parahippocampal Cortex. In addition, post-hoc analysis results and functional connectivity values for Left Parahippocampal Cortex-CA1, Left Subiculum-Retrosplenial Cortex, Right Posterior Cingulate Cortex-Anterior Cingulate Cortex, and Right Parahippocampal Cortex-Retrosplenial Cortex are shown using violin plots. *L*: Left; *R*: Right; *PCC*: Posterior Cingulate Cortex; *PHC*: Parahippocampal Cortex; *ACC*: Anterior Cingulate Cortex; *SUB*: Subiculum; *RSC*: Retrosplenial Cortex; *CA*: Cornu Ammonis; *SCI*: Subjective memory impairment; *MCI*: Mild cognitive impairment; *ADD*: Alzheimer's disease dementia. P-values were corrected for multiple comparisons using the False Discovery Rate correction. * $p < 0.05$; ** $p < 0.01$.

Table 2
ROI-restricted TBSS results.

Region	Cluster	Voxel Size	Peak Coordinate (MNI)			*F*	*p*	η^2
			x	y	z			
Fornix	Cluster 1	130	2	−6	11	15.55	0.015	0.245
R vCing	Cluster 1	182	28	−23	−24	12.02	0.010	0.257
L vCing	Cluster 1	24	−21	−33	−14	5.42	0.045	0.213
	Cluster 2	24	−26	−25	−23	4.40	0.045	0.165
	Cluster 3	42	−21	−17	−27	6.55	0.042	0.201

L: Left; *R*: Right; *vCing*: Ventral cingulum; *ROI*: Region of Interest; *TBSS*: Tract-Based Spatial Statistics. P-values were corrected for multiple comparisons using the False Discovery Rate correction. Partial eta square values have been reported. The significance threshold was set at $p < 0.05$.

among the three groups was completely replicated in the ADD vs SCI pairwise comparison accounting for the cumulative character of these functional disconnections along the disease progression. However, pairwise group comparisons extended this overall picture by revealing that the decreased FC of the right PHC – RSC represents the earliest change of the Papez circuit occurring in the MCI stage, while the FC decrease in the left PHC – CA1 specifically occurred later at the ADD stage. Additionally, SC analyses revealed a clear effect for the fornix, in addition to the loss of the white matter integrity along the right and left ventral cingulum bundles, which is in line with other reports in the literature (Berron et al., 2020; Kantarci et al., 2017; Metzler-Baddeley et al., 2012; Ray et al., 2015). However, the post-hoc analyses revealed that significant SC changes were present in the SCI vs ADD and MCI vs ADD comparisons, pointing to a later development of the WM changes compared with the FC changes. This point is further supported by the correlation analyses between each of the significantly affected FC and SC variables presented in Tables A3 in the Appendix, which shows that the FC changes with a significant progression from the SCI to ADD stage are correlated with a large number of SC decreases, while the FC decrease between the left PHC and CA1, which is introduced earliest in the ADD stage, is not correlated with any of the SC decreases.

As both FC and SC changes were significantly differing between specific stages of the disease, the next step of the analysis aimed the multimodal integration of both neuroimaging modalities for a better description of the disease progress. In order to evaluate the efficiency of the FC and SC differences in the discrimination of the specific clinical stages of the disease, a series of stepwise LDA between pairs of disease stages were performed. Considering

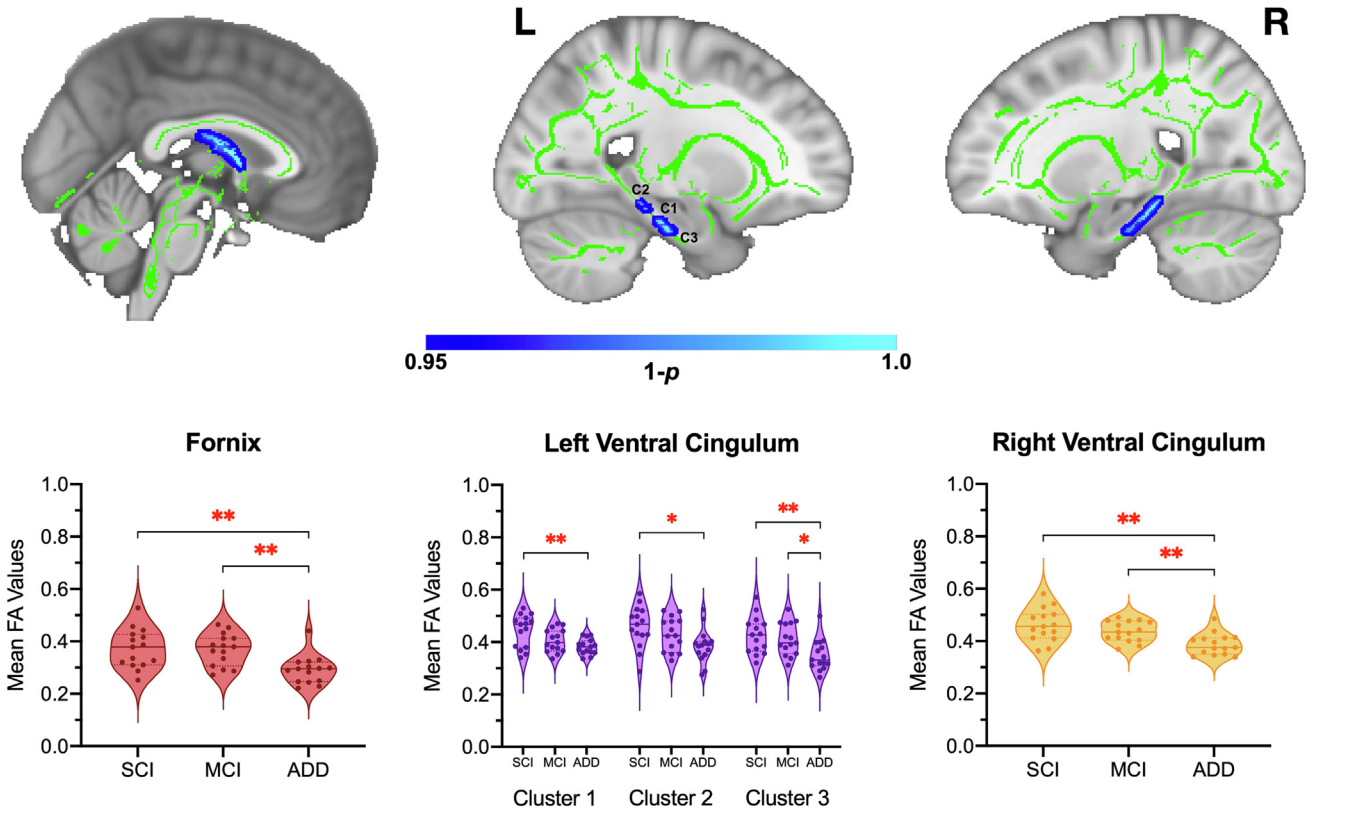


Fig. 5. Regions of interest that show significant fractional anisotropy differences in tract-based spatial statistics analysis (blue) overlayed on brain template (FSL HCP1065 FA 1 mm) and skeletonized mean fractional anisotropy mask (green). The color bar represents corrected 1-p values. *L*: Left; *R*: Right; *C*: Cluster; *SCI*: Subjective memory impairment; *MCI*: Mild cognitive impairment; *ADD*: Alzheimer's disease dementia. P-values were corrected for multiple comparisons using the False Discovery Rate correction. * $p < 0.05$; ** $p < 0.01$.

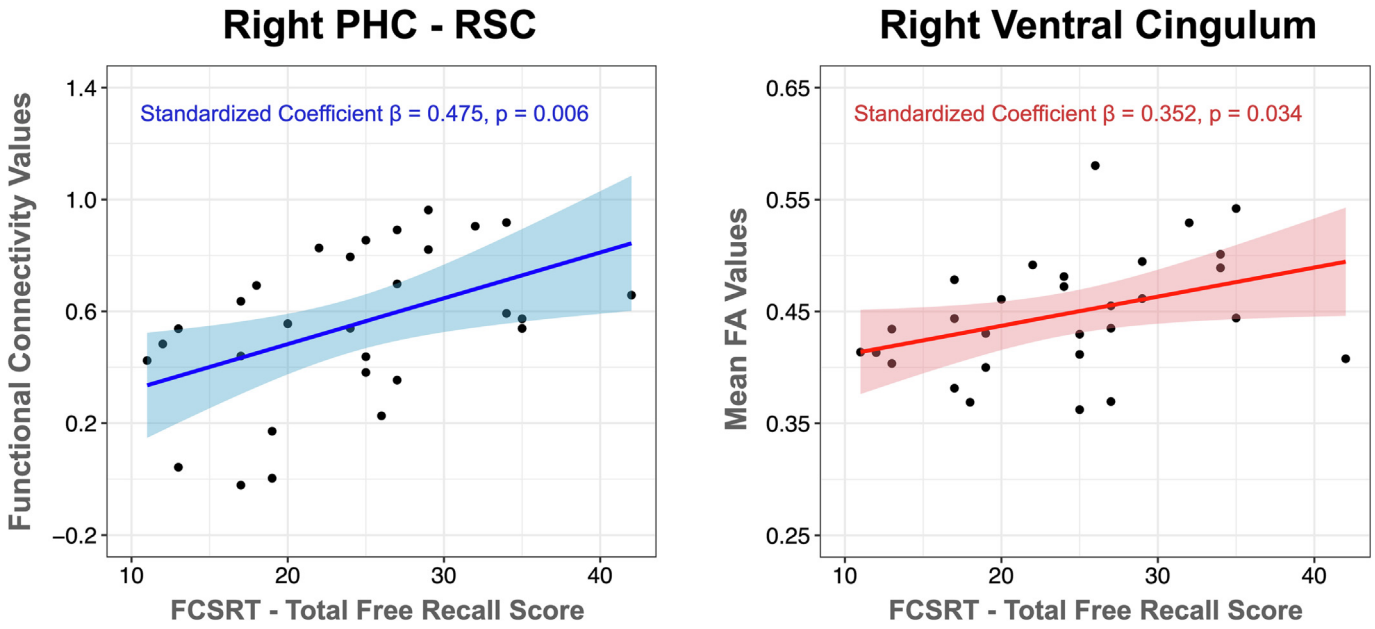


Fig. 6. Linear regression between the Free and Cued Selective Reminding Test – Total Free Recall scores and the functional and structural connectivity results of the subjective cognitive impairment and mild cognitive impairment groups. *PHC*: Parahippocampal Cortex; *RSC*: Retrosplenial Cortex; *FA*: Fractional Anisotropy; *L*:Left; *FCSRT:* Free and Cued Selective Reminding Test. The significance threshold was set at $p < 0.05$.

that the critical connectivity features for the different stages of the disease correspond to distinct parts of the Papez circuit, we preferred to run separate LDA for each pair of the disease stages instead of applying a multi-class scenario. These analyses revealed that the reduced FC between the right PHC and RSC was the only variable that discriminated the MCI from the SCI group with an

acceptable accuracy of 70%, while ADD group could be discriminated from each of the MCI and SCI groups with a high accuracy of 83.3% by two pairs of FC and SC variables. The reduced FC between the right PHC and RSC and the reduced integrity of the right ventral cingulum separated the ADD from the SCI group, while the reduced FC between the left PHC and CA1 and reduced fornix integrity separated the ADD from the MCI group. The ROC curves for each LDA are displayed in Fig. A1 in the Appendix. This pattern of the progression of the multimodal connectivity changes displays that the early stage of the disease is characterized by a functional disconnectivity between the PHC and RSC. The functional disconnectivity between the PHC and CA1 and the changes in the two important WM tracts of the Papez circuit, the ventral cingulum and the fornix, seem to mostly contribute to the dementia stage of the disease.

In order to test this pattern further at a finer scale in association with the neuropsychological performance, we performed a linear regression analysis to find out the multimodal connectivity variables that can predict the memory performance in the non-demented stages of the disease. Assuming that the between-group comparisons might be insensitive to slow progressive changes that might occur in any connectivity variable, we included all investigated FC and SC variables in the linear regression analysis. The forward stepwise multiple linear regression carried out on SCI and MCI participants revealed that the FC between the right PHC and RSC and the mean FA of the right ventral cingulum were the only two variables that might predict 28.1% of the variance of the FCSRT-TFR scores. These results nicely fit to the results of the previous between-group comparisons and the linear discriminant analyses in terms of an early affection of the FC between the PHC and RSC, but also extend them in terms of a rather slow progressive decrease of the integrity of the ventral cingulum in the early stages of the disease continuum.

The DMN has been the focus of the functional neuroimaging studies on AD due to its overlap with areas vulnerable to amyloid deposition (Buckner et al., 2008; Grieder et al., 2018; Pievani et al., 2014; Teipel et al., 2016). Based on the similarity of the resting-state temporal fluctuations of the BOLD signal of the HF with those of the DMN (Vincent et al., 2006), a group of studies have conceptualized the limbic structures centered around the HF as subcomponents of the DMN (Andrews-Hanna et al., 2010; Buckner et al., 2008), while other studies preferred to distinctively describe a limbic network (LN), which may show significant correlations with posterior DMN under specific conditions such as episodic memory retrieval (Golchert et al., 2017; Greicius et al., 2004; Teipel et al., 2016). This distinction is also reflected in the classification of the cerebral cortex into seven networks by Yeo and coworkers (2011) referenced in many recent human FC studies, which also address HF-centered structures as a separate LN. Our approach focusing on the Papez circuit instead of the nodes of the ICNs such as DMN or LN revealed decreased FCs between PCC and ACC and between PHC and RSC in the right hemisphere and between SUB and RSC and between PHC and CA1 in the left hemisphere, which are also important nodes of the DMN and LN. Therefore, the present results can also be discussed within the framework of ICN-based literature. Specifically, the reduced connectivities of the RSC, a critical intermediate region between the posterior DMN and HF (Ash et al., 2016; Kaboodvand et al., 2018), with the PHC and SUB are in accordance with the early concept that the FC deterioration in AD is particularly evident in the FC of the posterior DMN with the HF (Greicius et al., 2004). A meta-analysis examining various ICNs in AD reported a consistent decrease in the FC of the DMN, LN and salience network (SN) nodes selectively (Badhwar et al., 2017). Hence, our overall result supports the importance of the between-network connectivities between the posterior DMN and LN structures in ADC.

Within this context, the localization of the earliest FC difference between the RSC and PHC in comparing the SCI and MCI groups provides an interesting insight into the evolution of functional disconnectivities in ADC. The current viewpoint on the spread of the pathological processes in ADC relies on the different anatomical origins of the Aβ and tau pathologies, while the overlap of the tau pathology with the Aβ accumulation seems to result in the critical pathological progression in ADC (van der Kant et al., 2020; Masters et al., 2015). According to Jacobs et al. (2018), the amyloid contributes to the increased spreading of tau via the hippocampal or ventral cingulum bundle towards posterior cingulate areas, most probably leading to increased tau-related memory decline (Jacobs et al., 2018). Very recently, Lee et al. (2022) suggested two critical events that drive the cortical spreading of tau pathology in AD. The first is the deposition of NFTs in the lateral ERC driven by the cortical Aβ via remote connections, most probably involving ventral cingulum bundle (Lee et al., 2022). The second is the local convergence of Aβ and tau in the inferior temporal cortex that induces widespread and accelerated tau spreading to the neocortical areas of the brain which may then drive the development of dementia in AD (Lee et al., 2022). From this point of view, our results suggest that the connection between the RSC and PHC through the ventral cingulum seems to be the critical connection, where one of the earliest collisions between the spreads of the two pathologies occurs. The significant FC difference obtained between the PHC and RSC in the MCI compared with the SCI subjects in contrast to the development of a statistically significant SC decline in the ventral cingulum later in ADD stage points to the higher sensitivity of the FC to this early process. Nonetheless, the significant regression of the memory performance with the mean FA of the ventral cingulum in non-demented subjects provides indirect evidence for the importance of this connectivity from a structural point of view.

The cingulum bundle and fornix, the basic connections of the Papez circuit, have been extensively studied along the ADC (Aggleton et al., 2016). In studies examining white matter pathways in ADC, the most repeated finding is about microstructural changes in the cingulum, specifically in the ventral cingulum bundle, for both MCI and ADD (Bozzali et al., 2012; Choo et al., 2010; Metzler-Baddeley et al., 2012; Wang et al., 2017; Yu et al., 2017). A meta-analysis by Yu et al. (2017) compared amnestic MCI with controls and examined 77 studies on microstructural changes in the white matter pathways of the whole brain, especially in the cingulum bundle, fornix, and medial temporal lobe pathways (Yu et al., 2017). This meta-analysis reported a consistent FA decrease mainly in the ventral cingulum bundle, fornix, and uncinate fasciculus. In the present study, focusing on the Papez circuit, both WM tracts of the circuit, the fornix, and cingulum, displayed a significant diffusivity decline in ADD stage. As we could not show a significant difference between the pre-clinical and prodromal stages of the disease continuum, we cannot make a direct statement about any differential temporal pattern of the influence of the AD pathology on these tracts. However, the significant regression of the ventral cingulum diffusivity to the memory performance despite the lack of similar regression for the fornix indirectly points to the prominent role of the ventral cingulum in the cognitive decline along the pre-dementia stage of ADC. Similar to our results, a high level of correlation between the memory performance of AD patients and FA and mean diffusivity values of the ventral cingulum bundle has been reported in various previous studies (Berron et al., 2020; Kantarci et al., 2017; Metzler-Baddeley et al., 2012; Ray et al., 2015; Yu et al., 2017). Metzler-Baddeley and coworkers (2012) reported that memory performance in healthy elderly is primarily associated with fornix integrity. In contrast, memory performance in MCI shows greater dependence on the integrity of the ventral cingulum bundle (Metzler-Baddeley et al.,

2012). Evaluating our results within the context of the FC and SC findings in the literature and the concept of the critical collision of Aβ and tau accumulations in ADC neuropathology point clearly to the important position of the disconnectivity between the RSC and PHC through the ventral cingulum in the early course of the disease.

Two memory systems have been proposed by Ranganath and Ritchey (2012). While the anterior temporal system, including the temporopolar cortex, lateral orbitofrontal cortex, and amygdala, is the entry portal for the information related to the semantic "what" information, including the affective and motivational significance of the objects, to the HF through the perirhinal cortex via the lateral ERC, the posterior medial system consisting of the Papez circuit and DMN components is the entry portal for the episodic, contextual, "where" or "when" information to the HF through the PHC and RSC via the medial ERC (Ranganath and Ritchey, 2012). As the Papez circuit adopted as the central framework of the present study by large overlaps with the posterior medial system, our findings point to the early effects of the AD neuropathology on the ventral connections within the posterior medial system in line with previous reports on the early scene-related memory impairments (Lee et al., 2006). Consistent with the account that the collision of the Aβ pathology starting in the neocortex of the midline structures with the tau pathology stemming from the limbic structures plays a critical role in the spread and effectiveness of the tau pathology to the posterior medial memory system, the present result on the early PHC – RSC functional disconnectivity may possibly explain the observation that the tau pathology is primarily associated with semantic processes. In contrast, the amyloid pathology, through its collision with the tau pathology in the ventral cingulum, is associated mainly with episodic and contextual memory processes (Grande et al., 2021; Maass et al., 2019). Finally, our result also points to the importance of using neuropsychological tests related to the contextual, episodic component of the memory recollection for increased sensitivity of the neuropsychological evaluation of the memory impairment in the ADC.

Another interesting result of the present study is that a manifest functional disconnectivity between the PHC and CA1 is characteristic of the dementia stage. Similarly, a recent study reported that the CA1 was the only subregion that exhibited reduced FC in ADD compared with MCI patients (Yan et al., 2020). Considering evident volume loss in the CA1 sector in the early stage of the disease as reported in a series of volumetric studies (Hari et al., 2022; Zhao et al., 2019), present result on the relatively saved FC between the CA1 and PHC in the MCI stage seems to contradict the anatomic degeneration pattern. This can be an important result pointing to the effort of CA1 to compensate for the volume reduction in the early stage of the ADC, which, however, cannot be further compensated after progressive degeneration later in the course of the disease. Although the protection of the FC of CA1 cannot be simply associated with the increased activation of the CA1 neurons, reports on hyperactivity in the CA1 region in the MCI stage (Tran et al., 2017) can be considered a supporting finding for such compensatory activation.

5. Limitations

The relatively small number of subjects is the main limitation of the present study, which partly stems from selecting a subset of the subjects in the laboratory database such that the distribution of age and education are equalized among the three stages of the ADC. However, removing possible confounding effects of critical co-variates in the statistics, performing connectivity calculations in the subject space, and utilizing Monte-Carlo permutations with a high number of iterations can be considered strong measures to overcome this limitation. The absence of biomarkers of MCI vs SCI groups and the lack of longitudinal follow-up of the participants are other limitations of the study. We aim to improve future work by increasing the number of participants and using CSF biomarkers and clinical diagnostic criteria together in a longitudinal study design. Focusing on the nodes of the Papez circuit to scrutinize the FC and SC features of the episodic memory-related structures on a finer scale might have resulted by large in a predominance of the findings related to the posterior medial memory system, while an important part of the anterior temporal system was not directly included in the current analyses. Considering the recent neuroimaging works pointing to the anterior temporal memory system in the early identification of ADC, a detailed comparative analysis of the fine-scale connectivity patterns of both systems may extend present results in terms of enhancing the sensitivity of neuroimaging-based diagnostic criteria for the early stages of the disease.

6. Conclusion

In conclusion, while for the large-scale connections, the FC changes seem to precede manifest changes in SC as in the case of the reduced PHC – RSC FC, for short connections such as the CA1 – PHC, the FC is preserved until the dementia stage despite the observation of clear anatomic changes in CA1 volume in the early ADC stages. These results also highlight the importance of multimodal neuroimaging in search for biomarkers. Regarding the first finding, the collision of the Aβ plaques starting to accumulate in the neocortex and NFT accumulating in ERC in the ventral cingulum seem to affect the PHC – RSC FC, associated with memory decline in ADC, in an earlier stage before a manifest change in the SC is observable. The second important finding of the preserved CA1 – PHC FC in the MCI stage points to a possibly compensatory process in the already degenerated CA1 region. Additionally, the central role of the HF to DMN connectivity via PHC – RSC in the transmission of the episodic and contextual information along the posterior medial memory system points to the importance of shaping neuropsychological tests or task-based neuroimaging protocols that emphasize the contextual "where" or "when" information for the better-resolved evaluation of the ADC memory decline.

Funding

This work was supported by Istanbul University Research Projects Unit (Grant #: 2019 K12-149071); Istanbul University Research University Support Program (Grant #: TSA-2022–39128).

Conflict of interest

The authors declare no competing interests.

Ethical approval

The study was approved by the Clinical Research Ethics Committee of Istanbul University, Istanbul Faculty of Medicine (Protocol Number: 2018/1503). This study was performed in accordance with the ethical principles of the latest version of the Declaration of Helsinki.

Informed consent

Written informed consent was provided by all participants.

Acknowledgements

We thank Burak Acar, Elif Yıldırım and Ezgi Soncu Büyükişcan for their contribution. This study was produced from Emre Hari's master thesis (No: 568219). Emre Hari is a PhD scholarship holder from the Council of Higher Education (CoHE) in the field of Human Brain and Neuroscience, which is one of the 100 national priority areas determined by CoHE within the scope of the 100/2000 Program.

Appendix A. Supplementary data

Supplementary data to this article can be found online at https://doi.org/10.1016/j.clinph.2023.06.008.

References

Acosta-Cabronero J, Nestor PJ. Diffusion tensor imaging in Alzheimer's disease: insights into the limbic-diencephalic network and methodological considerations. Front Aging Neurosci 2014;6:266. https://doi.org/10.3389/fnagi.2014.00266.

Aggleton JP. Looking beyond the hippocampus: old and new neurological targets for understanding memory disorders. Proc R Soc B Biol Sci 2014;281:20140565. https://doi.org/10.1098/rspb.2014.0565.

Aggleton JP, Nelson AJD, O'Mara SM. Time to retire the serial Papez circuit: Implications for space, memory, and attention. Neurosci Biobehav Rev 2022;104813. https://doi.org/10.1016/j.neubiorev.2022.104813.

Aggleton JP, Pralus A, Nelson AJD, Hornberger M. Thalamic pathology and memory loss in early Alzheimer's disease: moving the focus from the medial temporal lobe to Papez circuit. Brain 2016;139:1877–90. https://doi.org/10.1093/brain/aww083.

Andersson JLR, Sotiropoulos SN. An integrated approach to correction for off-resonance effects and subject movement in diffusion MR imaging. Neuroimage 2016;125:1063–78. https://doi.org/10.1016/j.neuroimage.2015.10.019.

Andrews-Hanna JR, Reidler JS, Sepulcre J, Poulin R, Buckner RL. Functional-anatomic fractionation of the brain's default network. Neuron 2010;65:550–62. https://doi.org/10.1016/j.neuron.2010.02.005.

Ash JA, Lu H, Taxier LR, Long JM, Yang Y, Stein EA, et al. Functional connectivity with the retrosplenial cortex predicts cognitive aging in rats. Proc Natl Acad Sci 2016;113:12286–91. https://doi.org/10.1073/pnas.1525309113.

Badhwar A, Tam A, Dansereau C, Orban P, Hoffstaedter F, Bellec P. Resting-state network dysfunction in Alzheimer's disease: a systematic review and meta-analysis. Alzheimers Dement (Amst) 2017;8:73–85. https://doi.org/10.1016/j.dadm.2017.03.007.

Benjamini Y, Hochberg Y. Controlling the false discovery rate: a practical and powerful approach to multiple testing. J Roy Statist Soc Ser B 1995;57:289–300. https://doi.org/10.1111/j.2517-6161.1995.tb02031.x.

Berron D, van Westen D, Ossenkoppele R, Strandberg O, Hansson O. Medial temporal lobe connectivity and its associations with cognition in early Alzheimer's disease. Brain 2020;143:1233–48. https://doi.org/10.1093/brain/awaa068.

Bozzali M, Giulietti G, Basile B, Serra L, Spano B, Perri R, et al. Damage to the cingulum contributes to Alzheimer's disease pathophysiology by deafferentation mechanism. Hum Brain Mapp 2012;33:1295–308. https://doi.org/10.1002/hbm.21287.

Braak H, Braak E. Staging of Alzheimer's disease-related neurofibrillary changes. Neurobiol Aging 1995;16:271–84. https://doi.org/10.1016/0197-4580(95)00021-6.

Braak H, Braak E. Neuropathological stageing of Alzheimer-related changes. Acta Neuropathol 1991;82:239–59. https://doi.org/10.1007/BF00308809.

Braak H, Del Tredici K. Where, when, and in what form does sporadic Alzheimer's disease begin? Curr Opin Neurol 2012;25:708–14. https://doi.org/10.1097/WCO.0b013e32835a3432.

Bubb EJ, Kinnavane L, Aggleton JP. Hippocampal–diencephalic–cingulate networks for memory and emotion: an anatomical guide. Brain Neurosci Adv 2017;1. https://doi.org/10.1177/2398212817723443 2398212817723443.

Buckner RL, Andrews-Hanna JR, Schacter DL. The brain's default network: anatomy, function, and relevance to disease. Ann N Y Acad Sci 2008;1124:1–38. https://doi.org/10.1196/annals.1440.011.

Buschke H. Cued recall in amnesia. J Clin Neuropsychol 1984;6:433–40. https://doi.org/10.1080/01688638408401233.

Catani M, Dell'Acqua F, De Schotten MT. A revised limbic system model for memory, emotion and behaviour. Neurosci Biobehav Rev 2013;37:1724–37. https://doi.org/10.1016/j.neubiorev.2013.07.001.

Chételat G. Multimodal neuroimaging in Alzheimer's disease: early diagnosis, physiopathological mechanisms, and impact of lifestyle. J Alzheimer's Dis 2018;64:S199–211. https://doi.org/10.3233/JAD-179920.

Choi S-H, Kim Y-B, Paek S-H, Cho Z-H. Papez circuit observed by in vivo human brain with 7.0 T MRI super-resolution track density imaging and track tracing. Front Neuroanat 2019;13:17. https://doi.org/10.3389/fnana.2019.00017.

Choo ILH, Lee DY, Oh JS, Lee JS, Lee DS, Song IC, et al. Posterior cingulate cortex atrophy and regional cingulum disruption in mild cognitive impairment and Alzheimer's disease. Neurobiol Aging 2010;31:772–9. https://doi.org/10.1016/j.neurobiolaging.2008.06.015.

Dale AM, Fischl B, Sereno MI. Cortical surface-based analysis. I. Segmentation and surface reconstruction. Neuroimage 1999;9:179–94. https://doi.org/10.1006/nimg.1998.0395.

Destrieux C, Fischl B, Dale A, Halgren E. Automatic parcellation of human cortical gyri and sulci using standard anatomical nomenclature. Neuroimage 2010;53:1–15. https://doi.org/10.1016/j.neuroimage.2010.06.010.

Fellgiebel A, Schermuly I, Gerhard A, Keller I, Albrecht J, Weibrich C, et al. Functional relevant loss of long association fibre tracts integrity in early Alzheimer's disease. Neuropsychologia 2008;46:1698–706. https://doi.org/10.1016/j.neuropsychologia.2007.12.010.

Filippini N, Rao A, Wetten S, Gibson RA, Borrie M, Guzman D, et al. Anatomically-distinct genetic associations of APOE ε4 allele load with regional cortical atrophy in Alzheimer's disease. Neuroimage 2009;44:724–8.

Fischl B, Liu A, Dale AM. Automated manifold surgery: constructing geometrically accurate and topologically correct models of the human cerebral cortex. IEEE Trans Med Imaging 2001;20:70–80. https://doi.org/10.1109/42.906426.

Fischl B, Salat DH, Busa E, Albert M, Dieterich M, Haselgrove C, et al. Whole brain segmentation: automated labeling of neuroanatomical structures in the human brain. Neuron 2002;33:341–55. https://doi.org/10.1016/s0896-6273(02)00569-x.

Fletcher E, Raman M, Huebner P, Liu A, Mungas D, Carmichael O, et al. Loss of fornix white matter volume as a predictor of cognitive impairment in cognitively normal elderly individuals. JAMA Neurol 2013;70:1389–95. https://doi.org/10.1001/jamaneurol.2013.3263.

Folstein MF, Folstein SE, McHugh PR. "Mini-mental state". A practical method for grading the cognitive state of patients for the clinician. J Psychiatr Res 1975;12:189–98. https://doi.org/10.1016/0022-3956(75)90026-6.

Forno G, Lladó A, Hornberger M. Going round in circles—The Papez circuit in Alzheimer's disease. Eur J Neurosci 2021;54:7668–87. https://doi.org/10.1111/ejn.15494.

Genovese CR, Lazar NA, Nichols T. Thresholding of statistical maps in functional neuroimaging using the false discovery rate. Neuroimage 2002;15:870–8. https://doi.org/10.1006/nimg.2001.1037.

Golchert J, Smallwood J, Jefferies E, Seli P, Huntenburg JM, Liem F, et al. Individual variation in intentionality in the mind-wandering state is reflected in the integration of the default-mode, fronto-parietal, and limbic networks. Neuroimage 2017;146:226–35. https://doi.org/10.1016/j.neuroimage.2016.11.025.

Grande X, Berron D, Maass A, Bainbridge WA, Düzel E. Content-specific vulnerability of recent episodic memories in Alzheimer's disease. Neuropsychologia 2021;160. https://doi.org/10.1016/j.neuropsychologia.2021.107976 107976.

Greicius MD, Srivastava G, Reiss AL, Menon V. Default-mode network activity distinguishes Alzheimer's disease from healthy aging: evidence from functional MRI. Proc Natl Acad Sci 2004;101:4637–42. https://doi.org/10.1073/pnas.0308627101.

Grieder M, Wang DJJ, Dierks T, Wahlund L-O, Jann K. Default mode network complexity and cognitive decline in mild Alzheimer's disease. Front Neurosci 2018;12:770. https://doi.org/10.3389/fnins.2018.00770.

Grober E, Sanders AE, Hall C, Lipton RB. Free and cued selective reminding identifies very mild dementia in primary care. Alzheimer Dis Assoc Disord 2010;24:284–90. https://doi.org/10.1097/WAD.0b013e3181cfc78b.

Hampel H, Hardy J, Blennow K, Chen C, Perry G, Kim SH, et al. The amyloid-β pathway in Alzheimer's disease. Mol Psychiatry 2021;26:5481–503. https://doi.org/10.1038/s41380-021-01249-0.

Hari E, Kurt E, Bayram A, Kizilates-Evin G, Acar B, Demiralp T, et al. Volumetric changes within hippocampal subfields in Alzheimer's disease continuum. Neurol Sci 2022:1–9. https://doi.org/10.1007/s10072-022-05890-7.

Honda Y, Shibata H. Organizational connectivity among the CA1, subiculum, presubiculum, and entorhinal cortex in the rabbit. J Comp Neurol 2017;525:3705–41. https://doi.org/10.1002/cne.24297.

Hothorn T, Bretz F, Westfall P. Simultaneous inference in general parametric models. Biometrical J J Math Methods Biosci 2008;50:346–63. https://doi.org/10.1002/bimj.200810425.

Huang J, Auchus AP. Diffusion tensor imaging of normal appearing white matter and its correlation with cognitive functioning in mild cognitive impairment and Alzheimer's disease. Ann N Y Acad Sci 2007;1097:259–64. https://doi.org/10.1196/annals.1379.021.

Hubbard CS, Becerra L, Heinz N, Ludwick A, Rasooly T, Yendiki A, et al. Microstructural white matter abnormalities in the dorsal cingulum of adolescents with IBS. Eneuro 2018;5. https://doi.org/10.1523/ENEURO.0354-17.2018.

Iglesias JE, Augustinack JC, Nguyen K, Player CM, Player A, Wright M, et al. A computational atlas of the hippocampal formation using ex vivo, ultra-high resolution MRI: Application to adaptive segmentation of in vivo MRI. Neuroimage 2015;115:117–37. https://doi.org/10.1016/j.neuroimage.2015.04.042.

Iglesias JE, Insausti R, Lerma-Usabiaga G, Bocchetta M, Van Leemput K, Greve DN, et al. A probabilistic atlas of the human thalamic nuclei combining ex vivo MRI and histology. Neuroimage 2018;183:314–26. https://doi.org/10.1016/j.neuroimage.2018.08.012.

Ivnik RJ, Smith GE, Lucas JA, Tangalos EG, Kokmen E, Petersen RC. Free and cued selective reminding test: MOANS norms. J Clin Exp Neuropsychol 1997;19:676–91. https://doi.org/10.1080/01688639708403753.
Jacobs HIL, Hedden T, Schultz AP, Sepulcre J, Perea RD, Amariglio RE, et al. Structural tract alterations predict downstream tau accumulation in amyloid-positive older individuals. Nat Neurosci 2018;21:424–31. https://doi.org/10.1038/s41593-018-0070-z.
Jankowski MM, Ronnqvist KC, Tsanov M, Vann SD, Wright NF, Erichsen JT, et al. The anterior thalamus provides a subcortical circuit supporting memory and spatial navigation. Front Syst Neurosci 2013;7:45. https://doi.org/10.3389/fnsys.2013.00045.
Jenkinson M, Bannister P, Brady M, Smith S. Improved optimization for the robust and accurate linear registration and motion correction of brain images. Neuroimage 2002;17:825–41. https://doi.org/10.1006/nimg.2002.1132.
Jenkinson M, Smith S. A global optimisation method for robust affine registration of brain images. Med Image Anal 2001;5:143–56. https://doi.org/10.1016/S1361-8415(01)00036-6.
Jessen F, Wolfsgruber S, Wiese B, Bickel H, Mösch E, Kaduszkiewicz H, et al. AD dementia risk in late MCI, in early MCI, and in subjective memory impairment. Alzheimers Dement 2014;10:76–83. https://doi.org/10.1016/j.jalz.2012.09.017.
Kaboodvand N, Bäckman L, Nyberg L, Salami A. The retrosplenial cortex: A memory gateway between the cortical default mode network and the medial temporal lobe. Hum Brain Mapp 2018;39:2020–34. https://doi.org/10.1002/hbm.23983.
Kalus P, Slotboom J, Gallinat J, Mahlberg R, Cattapan-Ludewig K, Wiest R, et al. Examining the gateway to the limbic system with diffusion tensor imaging: the perforant pathway in dementia. Neuroimage 2006;30:713–20. https://doi.org/10.1016/j.neuroimage.2005.10.035.
Kantarci K, Murray ME, Schwarz CG, Reid RI, Przybelski SA, Lesnick T, et al. White-matter integrity on DTI and the pathologic staging of Alzheimer's disease. Neurobiol Aging 2017;56:172–9. https://doi.org/10.1016/j.neurobiolaging.2017.04.024.
Krauth A, Blanc R, Poveda A, Jeanmonod D, Morel A, Székely G. A mean three-dimensional atlas of the human thalamus: generation from multiple histological data. Neuroimage 2010;49:2053–62. https://doi.org/10.1016/j.neuroimage.2009.10.042.
La Joie R, Landeau B, Perrotin A, Bejanin A, Egret S, Pélerin A, et al. Intrinsic connectivity identifies the hippocampus as a main crossroad between Alzheimer's and semantic dementia-targeted networks. Neuron 2014;81:1417–28. https://doi.org/10.1016/j.neuron.2014.01.026.
Lee ACH, Buckley MJ, Gaffan D, Emery T, Hodges JR, Graham KS. Differentiating the roles of the hippocampus and perirhinal cortex in processes beyond long-term declarative memory: a double dissociation in dementia. J Neurosci 2006;26:5198–203. https://doi.org/10.1523/JNEUROSCI.3157-05.2006.
Lee WJ, Brown JA, Kim HR, La Joie R, Cho H, Lyoo CH, et al. Regional Aβ-tau interactions promote onset and acceleration of Alzheimer's disease tau spreading. Neuron 2022. https://doi.org/10.1016/j.neuron.2022.03.034.
Lemos R, Simões MR, Santiago B, Santana I. The free and cued selective reminding test: Validation for mild cognitive impairment and A lzheimer's disease. J Neuropsychol 2015;9:242–57. https://doi.org/10.1111/jnp.12048.
Maass A, Berron D, Harrison TM, Adams JN, La Joie R, Baker S, et al. Alzheimer's pathology targets distinct memory networks in the ageing brain. Brain 2019;142:2492–509. https://doi.org/10.1093/brain/awz154.
Masters CL, Bateman R, Blennow K, Rowe CC, Sperling RA, Cummings JL. Alzheimer's disease. Nat Rev Dis Prim 2015;1. https://doi.org/10.1038/nrdp.2015.56 15056.
McKhann GM, Knopman DS, Chertkow H, Hyman BT, Jack CRJ, Kawas CH, et al. The diagnosis of dementia due to Alzheimer's disease: recommendations from the National Institute on Aging-Alzheimer's Association workgroups on diagnostic guidelines for Alzheimer's disease. Alzheimers Dement 2011;7:263–9. https://doi.org/10.1016/j.jalz.2011.03.005.
Metzler-Baddeley C, Hunt S, Jones DK, Leemans A, Aggleton JP, O'Sullivan MJ. Temporal association tracts and the breakdown of episodic memory in mild cognitive impairment. Neurology 2012;79:2233–40. https://doi.org/10.1212/WNL.0b013e31827689e8.
Molinuevo JL, Rabin LA, Amariglio R, Buckley R, Dubois B, Ellis KA, et al. Implementation of subjective cognitive decline criteria in research studies. Alzheimers Dement 2017;13:296–311. https://doi.org/10.1016/j.jalz.2016.09.012.
Morris JC. The Clinical Dementia Rating (CDR). Neurology 1993;43:2412. https://doi.org/10.1212/WNL.43.11.2412-a.
Papez JW. A proposed mechanism of emotion. Arch Neurol Psychiatry 1937;38:725–43. https://doi.org/10.1001/archneurpsyc.1937.02260220069003.
Petersen RC. Mild cognitive impairment as a diagnostic entity. J Intern Med 2004;256:183–94. https://doi.org/10.1111/j.1365-2796.2004.01388.x.
Pievani M, Filippini N, Van Den Heuvel MP, Cappa SF, Frisoni GB. Brain connectivity in neurodegenerative diseases—from phenotype to proteinopathy. Nat Rev Neurol 2014;10:620–33. https://doi.org/10.1038/nrneurol.2014.178.
Raichle ME, MacLeod AM, Snyder AZ, Powers WJ, Gusnard DA, Shulman GL. A default mode of brain function. Proc Natl Acad Sci 2001;98:676–82. https://doi.org/10.1073/pnas.98.2.676.
Raj A, Kuceyeski A, Weiner M. A network diffusion model of disease progression in dementia. Neuron 2012;73:1204–15. https://doi.org/10.1016/j.neuron.2011.12.040.
Ranganath C, Ritchey M. Two cortical systems for memory-guided behaviour. Nat Rev Neurosci 2012;13:713–26. https://doi.org/10.1038/nrn3338.
Ray NJ, Metzler-Baddeley C, Khondoker MR, Grothe MJ, Teipel S, Wright P, et al. Cholinergic basal forebrain structure influences the reconfiguration of white matter connections to support residual memory in mild cognitive impairment. J Neurosci 2015;35:739–47. https://doi.org/10.1523/JNEUROSCI.3617-14.2015.
Roberts RO, Geda YE, Knopman DS, Cha RH, Pankratz VS, Boeve BF, et al. The Mayo Clinic Study of Aging: design and sampling, participation, baseline measures and sample characteristics. Neuroepidemiology 2008;30:58–69. https://doi.org/10.1159/000115751.
Saka E, Mihci E, Topcuoglu MA, Balkan S. Enhanced cued recall has a high utility as a screening test in the diagnosis of Alzheimer's disease and mild cognitive impairment in Turkish people. Arch Clin Neuropsychol 2006;21:745–51. https://doi.org/10.1016/j.acn.2006.08.007.
Sanabria-Castro A, Alvarado-Echeverría I, Monge-Bonilla C. Molecular Pathogenesis of Alzheimer's Disease: An Update. Ann Neurosci 2017;24:46–54. https://doi.org/10.1159/000464422.
Schultz C, Engelhardt M. Anatomy of the hippocampal formation. Front Neurol Neurosci 2014;34:6–17. https://doi.org/10.1159/000360925.
Seeley WW, Crawford RK, Zhou J, Miller BL, Greicius MD. Neurodegenerative diseases target large-scale human brain networks. Neuron 2009;62:42–52. https://doi.org/10.1016/j.neuron.2009.03.024.
Sexton CE, Mackay CE, Lonie JA, Bastin ME, Terrière E, O'Carroll RE, et al. MRI correlates of episodic memory in Alzheimer's disease, mild cognitive impairment, and healthy aging. Psychiatry Res Neuroimaging 2010;184:57–62. https://doi.org/10.1016/j.pscychresns.2010.07.005.
Smith SM. Fast robust automated brain extraction. Hum Brain Mapp 2002;17:143–55. https://doi.org/10.1002/hbm.10062.
Smith SM, Jenkinson M, Johansen-Berg H, Rueckert D, Nichols TE, Mackay CE, et al. Tract-based spatial statistics: voxelwise analysis of multi-subject diffusion data. Neuroimage 2006;31:1487–505. https://doi.org/10.1016/j.neuroimage.2006.02.024.
Smith SM, Jenkinson M, Woolrich MW, Beckmann CF, Behrens TEJ, Johansen-Berg H, et al. Advances in functional and structural MR image analysis and implementation as FSL. Neuroimage 2004;23:S208–19. https://doi.org/10.1016/j.neuroimage.2004.07.051.
Smith SM, Nichols TE. Threshold-free cluster enhancement: addressing problems of smoothing, threshold dependence and localisation in cluster inference. Neuroimage 2009;44:83–98. https://doi.org/10.1016/j.neuroimage.2008.03.061.
Staffaroni AM, Brown JA, Casaletto KB, Elahi FM, Deng J, Neuhaus J, et al. The longitudinal trajectory of default mode network connectivity in healthy older adults varies as a function of age and is associated with changes in episodic memory and processing speed. J Neurosci 2018;38:2809–17. https://doi.org/10.1523/JNEUROSCI.3067-17.2018.
Supekar K, Menon V, Rubin D, Musen M, Greicius MD. Network analysis of intrinsic functional brain connectivity in Alzheimer's disease. PLoS Comput Biol 2008;4:e1000100.
Teichmann M, Epelbaum S, Samri D, Nogueira ML, Michon A, Hampel H, et al. Free and Cued Selective Reminding Test–accuracy for the differential diagnosis of Alzheimer's and neurodegenerative diseases: a large-scale biomarker-characterized monocenter cohort study (ClinAD). Alzheimer's Dement 2017;13:913–23. https://doi.org/10.1016/j.jalz.2016.12.014.
Teipel S, Grothe MJ, Zhou J, Sepulcre J, Dyrba M, Sorg C, et al. Measuring cortical connectivity in Alzheimer's disease as a brain neural network pathology: toward clinical applications. J Int Neuropsychol Soc 2016;22:138–63. https://doi.org/10.1017/S1355617715000995.
Tomczak M, Tomczak E. The need to report effect size estimates revisited. An overview of some recommended measures of effect size. Trends Sport Sci 2014;1:19–25.
Tran TT, Speck CL, Pisupati A, Gallagher M, Bakker A. Increased hippocampal activation in ApoE-4 carriers and non-carriers with amnestic mild cognitive impairment. NeuroImage Clin 2017;13:237–45. https://doi.org/10.1016/j.nicl.2016.12.002.
van der Kant R, Goldstein LSB, Ossenkoppele R. Amyloid-β-independent regulators of tau pathology in Alzheimer disease. Nat Rev Neurosci 2020;21:21–35. https://doi.org/10.1038/s41583-019-0240-3.
Villemagne VL, Ong K, Mulligan RS, Holl G, Pejoska S, Jones G, et al. Amyloid imaging with 18F-florbetaben in Alzheimer disease and other dementias. J Nucl Med 2011;52:1210–7. https://doi.org/10.2967/jnumed.111.089730.
Vincent JL, Snyder AZ, Fox MD, Shannon BJ, Andrews JR, Raichle ME, et al. Coherent spontaneous activity identifies a hippocampal-parietal memory network. J Neurophysiol 2006;96:3517–31. https://doi.org/10.1152/jn.00048.2006.
Wang P, Zhou B, Yao H, Zhan Y, Zhang Z, Cui Y, et al. Aberrant intra-and inter-network connectivity architectures in Alzheimer's disease and mild cognitive impairment. Sci Rep 2015;5:1–12. https://doi.org/10.1038/srep14824.
Wang Z, Dai Z, Shu H, Liu D, Guo Q, He Y, et al. Cortical thickness and microstructural white matter changes detect amnestic mild cognitive impairment. J Alzheimer's Dis 2017;56:415–28. https://doi.org/10.3233/JAD-160724.
Winkler AM, Ridgway GR, Webster MA, Smith SM, Nichols TE. Permutation inference for the general linear model. Neuroimage 2014;92:381–97. https://doi.org/10.1016/j.neuroimage.2014.01.060.
Xia M, Wang J, He Y. BrainNet Viewer: a network visualization tool for human brain connectomics. PLoS One 2013;8:7. https://doi.org/10.1371/journal.pone.0068910.
Yan S, Zheng C, Cui B, Qi Z, Zhao Z, An Y, et al. Multiparametric imaging hippocampal neurodegeneration and functional connectivity with

simultaneous PET/MRI in Alzheimer's disease. Eur J Nucl Med Mol Imaging 2020;47:2440–52. https://doi.org/10.1007/s00259-020-04752-8.

Yu J, Lam CLM, Lee TMC. White matter microstructural abnormalities in amnestic mild cognitive impairment: A meta-analysis of whole-brain and ROI-based studies. Neurosci Biobehav Rev 2017;83:405–16. https://doi.org/10.1016/j.neubiorev.2017.10.026.

Zhang Y, Schuff N, Jahng G-H, Bayne W, Mori S, Schad L, et al. Diffusion tensor imaging of cingulum fibers in mild cognitive impairment and Alzheimer disease. Neurology 2007;68:13–9. https://doi.org/10.1212/01.wnl.0000250326.77323.01.

Zhao W, Wang X, Yin C, He M, Li S, Han Y. Trajectories of the Hippocampal Subfields Atrophy in the Alzheimer's Disease: A Structural Imaging Study. Front Neuroinform 2019;13:13. https://doi.org/10.3389/fninf.2019.00013.

Zhuang L, Sachdev PS, Trollor JN, Kochan NA, Reppermund S, Brodaty H, et al. Microstructural white matter changes in cognitively normal individuals at risk of amnestic MCI. Neurology 2012;79:748–54. https://doi.org/10.1212/WNL.0b013e3182661f4d.